Seeded growth of ZIF-8 on the surface of carbon nanotubes towards self-supporting gas separation membranes — Source link ↗

Ludovic F. Dumée, Ludovic F. Dumée, Li He, Matthew R. Hill ...+8 more authors

Institutions: Victoria University, Australia, Deakin University, Commonwealth Scientific and Industrial Research Organisation, Monash University, Clayton campus

Topics: Gas separation, Membrane, Adsorption, Permeation and Carbon nanotube

Related papers:

- Exceptional chemical and thermal stability of zeolitic imidazolate frameworks

- The Chemistry and Applications of Metal-Organic Frameworks

- Highly Permeable Zeolite Imidazolate Framework-8 Membranes for CO2/CH4 Separation

- Oriented Zeolitic Imidazolate Framework-8 Membrane with Sharp H2/C3H8 Molecular Sieve Separation

- Synthesis of ceramic hollow fiber supported zeolitic imidazolate framework-8 (ZIF-8) membranes with high hydrogen permeability

Share this paper:

View more about this paper here: https://typeset.io/papers/seeded-growth-of-zif-8-on-the-surface-of-carbon-nanotubes-2wbeud7tgs

Deakin Research Online

Available from Deakin Research Online:

Seeded growth of ZIF-8 on the surface of carbon nanotubes towards self-supporting gas separation membranes†

Ludovic Dumée,‡*[ab] Li He,‡[a] Matthew Hill,[c] Bo Zhu,[b] Mikel Duke,[b] Jürg Schütz,[c] Fengshua She,[a] Huanting Wang,[d] Stephen Gray,[b] Peter Hodgson[a] and Lingxue Kong[a]

We report the synthesis of the first continuous, inter-grown ZIF-8 membrane *via* the secondary growth method. ZIF-8 crystals were seeded and strongly anchored onto porous carbon nanotube bucky-paper supports and hydrothermally grown into a dense and continuous ZIF-8 network. The self-supporting hybrid metal organic framework membranes were characterized by scanning electron microscopy and shown to exhibit both a very homogeneous structure and a very smooth nanotube-metal organic framework interface. Gas adsorption (H_2, CH_4, CO_2, N_2) and permeation (He, CO_2, N_2 and Xe) tests were performed to evaluate the permeance of each gas and to predict the selectivity. The membranes were highly robust and sustained pressures as high as 500 kPa. Furthermore, the high selectivity of N_2 over CO_2 and Xe (33 and 163 respectively), shown by gas adsorption single gas permeation and mixed gas permeation clearly demonstrates the near defect-free nature of the membranes while the high hydrothermal stability of ZIF-8 makes these novel composites highly promising for water vapour saturated gas treatment.

Introduction

Metal–organic frameworks (MOFs) have attracted considerable attention over the past 15 years for their ability to selectively separate gas mixtures by sub-nanometre molecular sieving.[1,2] MOFs are highly crystalline materials that can take a wide variety of morphologies and offer very specific functionalities and properties. Water stable MOFs, such as ZIF-8, used for gas separation or chemical sensing, typically have very large internal surface area (between 1300 and 1600 m^2 g^{-1} for ZIF-8 (ref. 3)), narrow micro-pore size distribution (around 3.4 Å for ZIF-8 (ref. 4)), and highly versatile surface chemistry. In fact, due to the presence of water vapour in most industrial processes, the development of robust and stable materials, such as water-resistant MOFs, are highly sought for gas separation, storage and carbon capture.[5,6] The mechanisms ruling MOFs growth lead to the formation of macro-monoliths whose size may reach tens to hundreds of micrometres.[2,7]

Recent efforts have focused on tailoring growth seeding and conditions to interconnect the monoliths and create denser and defect free crystal networks that can be used as self-supporting films.[8–11] Strategies to produce supported MOF thin films and membranes face key engineering challenges, including the control and optimization of the interface between the scaffold and the MOF crystals, as well as the homogeneous control of the growth mechanisms in confined spaces to fully benefit from the unique MOF properties.[7,12] Although the use of dense substrates, such as gold surfaces, silicon wafers, graphite, polymers or sapphire and their surface functionalization with specific functional groups were successful routes for generating thin MOF films,[7,13–15] promising trials with porous substrates have been largely limited to rigid, low porosity supports such as alumina or polymeric non-woven materials.[12,16] The growth of MOFs within a porous structure, as opposed to their incorporation into mixed matrix membranes,[2] was demonstrated to lead to the fabrication of membrane materials possessing enhanced mechanical stability and higher performance.[7,10,11]

However, challenges related to the fabrication of defect-free MOF membranes and to the control of the interface between the MOFs and the interstitial gaps within the structure have not been fully solved.[12,17] This is primarily related to the difficult control of the MOF initial growth steps, which corresponds to the adsorption of the metal ions, and to MOF crystal inter-connection and reticulation, progressively embedding the

[a]Institute for Frontier Materials, Deakin University, Pigdons Road, 3216 Waurn Ponds, Victoria, Australia. E-mail: ludovic.dumee@deakin.edu.au; Fax: +61 352271103; Tel: +61 410131312

[b]Institute for Sustainability and Innovation, College of Engineering and Science, Victoria University, Hoppers lane, 3030 Werribee, Victoria, Australia

[c]CSIRO Materials Science and Engineering, Private bag 10, 3168 Clayton South, Victoria, Australia

[d]Department of Chemical Engineering, Monash University, 3800, Clayton, Australia

† Electronic supplementary information (ESI) available. See DOI: 10.1039/c3ta11483j

‡ The two authors equally contributed to the manuscript and work.

supporting substrate. The specific surface area, the surface chemistry and the pore size distribution of the porous structures, must be well controlled to avoid voids remaining within the final membrane. Electro-spun webs[12] were recently successfully used for this purpose, but the large size of the pores and the low porosity of the structures remained limitations to the processing of highly interconnected and free-standing MOF hybrid structures.[10,17–19] Recently, MOF crystals were also *in situ* grown and confined into carbon nanotubes (CNTs) providing an enhanced material for gas adsorption.[20] The development of a new type of reinforced self-supporting defect free MOF membrane, exhibiting high gas permeability and high specific selectivity is, therefore, still required. A number of nano-porous structures have the potential to tackle these issues to process larger volume ratio MOF membranes with fewer defects. Amongst these candidates, carbon nanotube (CNT) buckypapers (BP) have already been demonstrated to be outstanding membrane materials for water desalination[21] or as scaffolds for gas adsorption.[22] The large range of surface functional groups that can be grafted onto CNT surfaces[23–25] as well as the small pore size (20–40 nm), high flexibility and compressibility and large porosity (>90%) of CNT BPs[26] are clear advantages for initiation of MOF growth from the graphene surface and within CNT BP interstitial pores.

In this research, ZIF-8 (ref. 27) nano-crystals were seeded and grown for the first time within CNT BPs to create a novel class of robust, defect-free, hybrid gas separation membranes. ZIF-8 was selected for its demonstrated high hydro-thermal stability, making it one of the most stable and promising MOF structures for complex gas and liquid separation applications.[8,9,16]

Results and discussion

The CNT BP substrates exhibited a homogeneous structure with a narrow pore size distribution ranging between 25 and 50 nm, depending on the diameter of the CNTs used to prepare the BPs.[26] Defect free membranes were prepared by growing ZIF-8 MOF homogeneously within the interstitial pores of the BP to form a continuous and dense network (Fig. 1a and b). ZIF-8 nano-crystals (Fig. 1e and f), formed by adsorption of zinc ions on the CNT surface, progressively grew to form a dense network within the nanotube matrix prior to growing across the BP (Fig. 1c). In addition, the size of the initial nano-crystals on the CNTs was around 200 nm, while the diameter of the ZIF-8 crystals on the BP surface was between 20 and 50 μm; very close to that reported by Yao *et al.*, 2011.[8] The cross sections shown in Fig. 1b and c clearly show that the hybrid membranes exhibit a continuous and homogeneous morphology across their entire thickness. As shown on Fig. 1c and d, the CNT–ZIF-8 crystal interface was also found to be very smooth and the CNTs were eventually completely embedded within the ZIF-8 matrix. Although defect free ZIF-8 membranes were prepared with both fine (10 nm) and coarse (40 nm) diameter CNTs (Table S2†), the coarse CNT BP exhibits a lower N_2 adsorption (Table 1 and Fig. S2†) and a lower mechanical strength.[26] This was previously reported and attributed to the larger diameter of coarser CNTs

which reduces both the specific surface area and the number of CNT–CNT contact points within the BP structure.[26]

The crystalline structure of the ZIF-8 was confirmed by XRD (Fig. 2 and S4†). Although, the presence of CNTs leads to a broad range of diffraction peaks between 12° and 17° (ref. 28) (Fig. 2a and b), ZIF-8 diffraction peak positions remain exactly the same as those of the ZIF-8 reference[29] sample without CNTs (Fig. 2c). It was previously demonstrated that a number of low intensity diffraction peaks present for randomly distributed CNTs could be attributed to the crystalline faces of graphite and graphene besides the main (0 0 2), (1 0 0) and (1 1 0) peaks.[30] The XRD results, therefore, confirm that contact between CNTs and ZIF-8 does not have any detrimental impact on the ZIF-8 growth and crystalline structure. Small Angle X-ray Scattering (SAXS) patterns and Wide Angle X-ray Scattering (WAXS) patterns were also acquired on ZIF-8s alone and hybrid membranes to assess of the quality of the structure and coherence of the crystals (Fig. 2d–f). As previously reported,[31] CNT assembled into a BP structure produced a broad SAXS scattering region around 0.05 and 0.085 $Å^{-1}$. This dispersity is due to the random nature of the CNT random distribution across the BP and to the addition of all SAXS patterns from differently oriented CNTs. The peaks visible for the ZIF-8 structure were found to be in very good agreement with recently reported ZIF-8 SAXS data (peaks at 0.54, 0.68, 0.75, 0.92 and 1.01 $Å^{-1}$) and WAXS data[32] (the Bragg reflections appearing on the WAXS patterns belong to the cubic body-centred lattice of ZIF-8 (ref. 32) (110, 200, 211, 220 and 310 and 222 over a q range of 0.1 to 1.4 $Å^{-1}$)).

Gas adsorption within the hybrid ZIF 8 was investigated to evaluate the strength of adhesion between gas molecules and the hybrid CNT–ZIF-8 matrix. The CNT–ZIF-8 membranes exhibited a high H_2 enthalpy of adsorption, with capacities up to 124.9 cm^3 g^{-1} (*i.e.* 1.5 wt%), very close to that reported for pure ZIF-8 crystals.[33] As shown in Table 1 and Fig. S3,† the volume of CO_2 adsorbed across the samples was larger than that of CH_4 which was previously attributed to the narrow bottle neck structure at the ZIF-8 pore entrance. As previously demonstrated[27] ZIF-8 crystalline structure is composed of large cavities (11.6 Å) inter-connected through much smaller apertures (3.4 Å). In addition, single gas permeation experiments were performed on a series of gas (Fig. 3). CO_2, despite having a kinetic diameter of only 3.3 Å and therefore being nearly 10% smaller than N_2, was found to permeate 34 times slower (kinetic diameter of 3.64 Å – see ESI†). This behaviour is attributed to the combined linear morphology and permanent dipole moment of CO_2 and to the peculiar structure of ZIF-8. The low CO_2 selectivity may also be related to non-fully crystallized 2-methyl imidazole molecules on the surface or within ZIF-8 crystals as this molecule is able to strongly coordinate with CO_2 gas.[16] In addition, except for CO_2, the inverse relationship between gas molecular weight and permeance shown in Fig. 3b suggests that the type of diffusion across the membrane was primarily dominated by Knudsen diffusion as heavier elements permeated more slowly across the membrane. The nature and integrity of the interface between ZIF-8 crystals and their surrounding matrix is critical to prepare defect-free
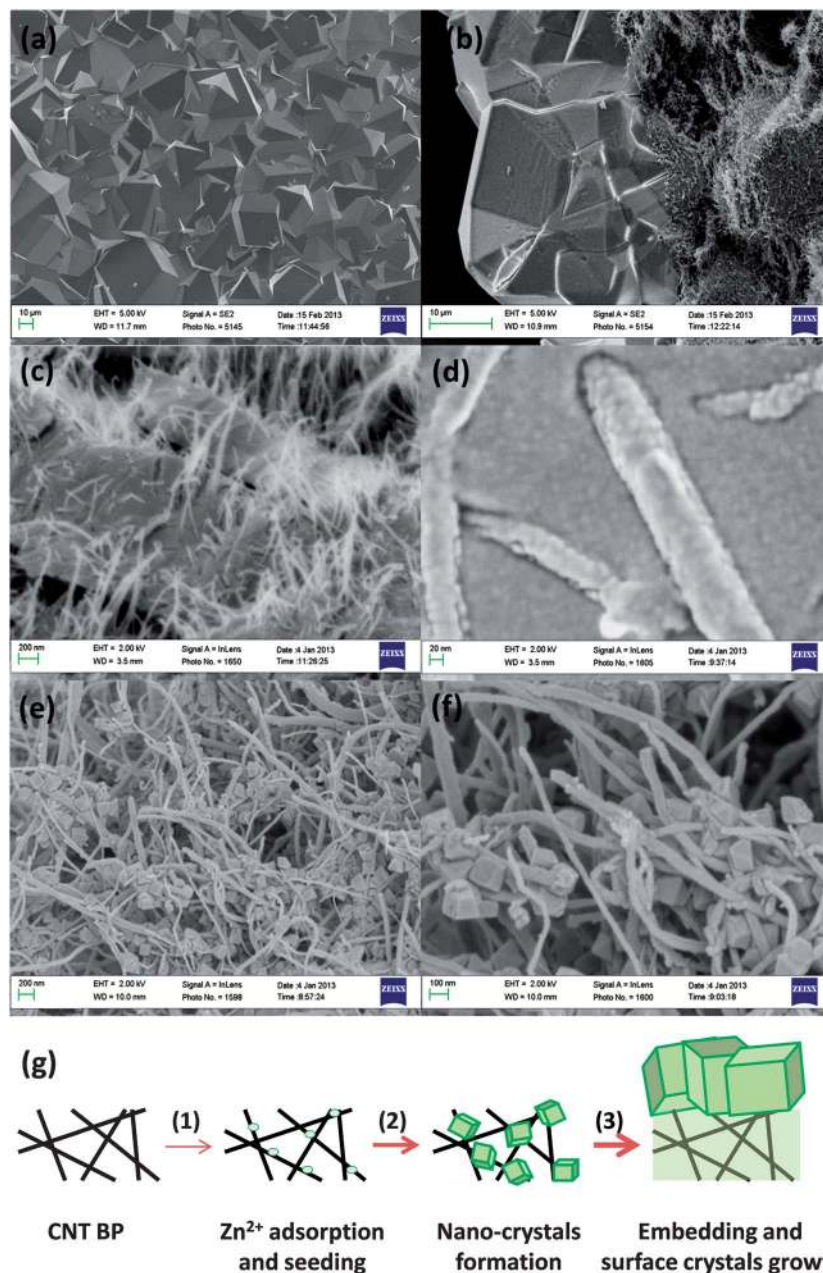
Fig. 1 SEM of the ZIF-8–CNT BP composite membranes; (a) top surface of the ZIF-8 hybrid membrane with clear macro-sized ZIF-8 crystals; (b) cross section view of ZIF-8 hybrid membrane; (c) embedded coarse CNTs within the ZIF-8 matrix; (d) view of a ZIF-8–CNT interface; (e) and (f) evidence of the formation of ZIF-8 nano-crystals on the CNTs during the early stage of ZIF-8 growth.

membranes, and is currently one of the main fields of MOF-composite fabrication investigation. The separation factor of He/N_2 obtained through the present work (2.5) is very close to the theoretical Knudsen separation index (2.64) corroborating that the membranes are near-defect free but that surface diffusion may occur between the massive ZIF-8 crystals as previously reported.[12] It is also noteworthy that despite having a kinetic diameter larger than the ZIF-8 pore size (3.64 Å against 3.4 Å), N_2 is able to permeate across the ZIF-8 membrane. This phenomenon was attributed to the simultaneous flexible nature of ZIF-8 crystals[34,35] and to diffusion at the interface between ZIF-8 crystals.[27] The dimension of these

defects at crystal boundaries has not been defined to date, but the very high N_2 selectivity against Xe suggests that its size should be smaller than 3.96 Å (Table S3 – ESI†) and therefore makes of the novel ZIF-8–CNT membranes very and stable structures for gas separation. The pore size distribution was very narrow, obtained from BET–BJH N_2 adsorption[9,10] on fragmented samples of membranes (Fig. 4), with an average pore size close to 1 nm which is very well correlated with the intrinsic bottle-neck micro-structure of ZIF-8. In addition, no major difference of permeation was found between the membranes made from CNTs of different diameters suggesting that the BP pore size does not

9210 | J. Mater. Chem. A, 2013, **1**, 9208–9214

This journal is © The Royal Society of Chemistry 2013

Table 1 BET surface area and gas adsorption (RTP) on the CNT BP and hybrid membrane composites; the specific surface area of ZIF-8 was shown to be close to 1496 m^2 g^{-1} (ref. 39)

| Property	Unit	Support		Hybrid membranes	
		Fine CNTs[26]	Coarse CNTs[26]	Fine CNTs + ZIF-8	Coarse CNTs + ZIF-8
N_2 specific surface area	m^2 g^{-1}	197.1	36	1650	1279
N_2 volume adsorption at 1 bar and 77 K	cm^3 g^{-1}	1.7 (ref. 22)	—	422.9	359.2
CH_4 volume adsorption at 1 bar and 273 K	cm^3 g^{-1}	—	—	7	5.72
CO_2 volume adsorption at 1 bar and 273 K	cm^3 g^{-1}	6.5 (ref. 22)	—	25.3	15.5
H_2 adsorption at 1 bar and 77 K	cm^3 g^{-1}	—	—	124.9	97.3
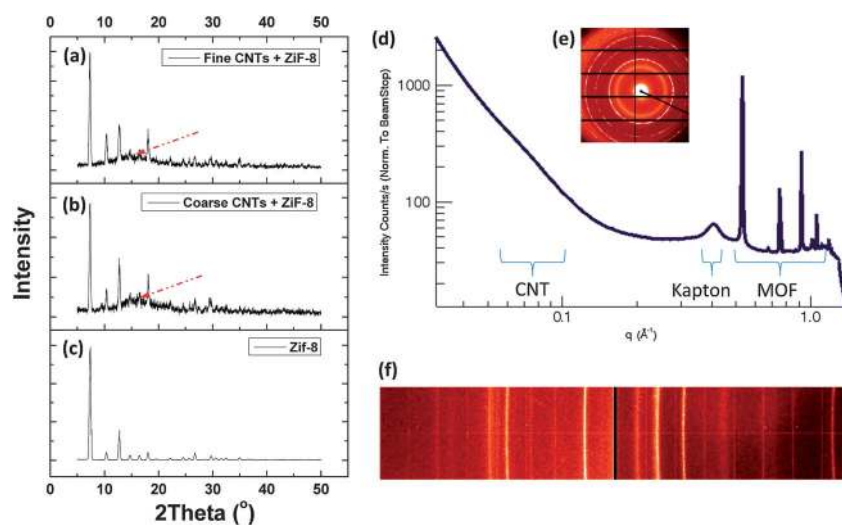
Fig. 2 XRD spectra of (a) hybrid fine CNTs and ZIF-8 membrane and (b) hybrid coarse CNTs and ZIF-8 membrane and (c) ZIF-8 alone. The broad absorption band (dotted red arrow) visible on (a) and (b) corresponds to the characteristic signature of randomly distributed CNTs;[30] (d) and (e) scattering spectra of the hybrid ZIF-8- thin CNT composites and corresponding scattering pattern, (f) WAXS signal acquired for the ZIF-8 crystals alone – sandwiched between Kapton tape. The main SAXS scattering peaks corresponding to the ZIF-8 crystalline structure, Kapton tape used for mounting and CNTs are indicated on the graph (SAXS peak at 0.4 Å^{-1}).

substantially affect the ZIF-8 crystal growth and that the interface CNT–ZIF-8 is homogenous even for larger CNTs. Furthermore, it is noteworthy that due to the large size of the CNT BP pores (~25 nm (ref. 22 and 26)) the support clearly does not play any role on the separation properties.

The N_2 adsorption and membrane separation performance of our hybrid membranes is also found to be superior to that previously reported. For the CNT BP–ZIF-8 membranes, the specific surface area of the membranes was 1.8 times larger than that reported for ZIF-8 grown on electro-spun webs.[12] This enhancement was attributed to the natural high specific surface area and aspect ratio of the CNTs which benefits the growth of ZIF-8 nano-crystals by creating a larger number of potential growth sites than previously reported for electro-spun nano-fibres.[12,19] The presence of the high surface area CNTs dramatically increases the density of nucleation sites per unit volume favouring the development of interconnected matrixes and better packing of the ZIF-8 nano-crystals (Fig. 1 and S1†). In addition, the permeation of these membranes falls within the highest reported values for this type of seeded growth within a

porous material.[11,36,37] The difference with previous publications is attributed to variations in the thickness of the ZIF-8 surface macro-crystals. In our case, this top layer was ~30 μm thick, and reducing the size of the ZIF-8 crystals would likely lead to higher permeation membranes. The nano-pores generated by the interstitial gaps between the CNTs within the BP structure, therefore, represent a highly promising environment in which to simultaneously stabilize the growth of MOF and enhance the materials specific surface area, a critical parameter in gas separation and storage.

The novel CNT–ZIF-8 hybrid membranes were also found to be able to sustain large pressure differentials (up to 500 kPa) without any loss of either integrity or selectivity (Fig. 3c). The compression resistance of the gas separation membranes is critical as industrial separation processes typically involve large feed to permeate pressure differences.[38] As shown in Fig. 3c, the permeance across the hybrid membranes for both N_2 and CO_2 increases linearly with absolute differential pressure (square regression coefficients of 0.9874 and 0.9852 for N_2 and CO_2, respectively). The membranes were also re-tested at
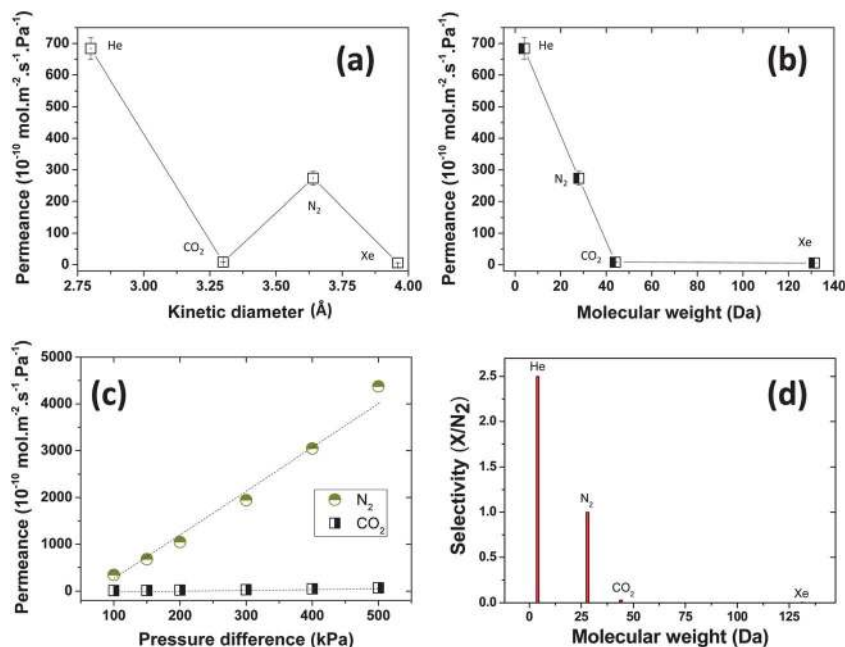
Fig. 3 Single gas permeation results across fine CNT–ZIF-8 and coarse CNT–ZIF-8 membranes; (A) and (B) correlation between gas permeance and the gas kinetic diameter at a pressure of 100 kPa (A) and molecular weight (B) for CO_2, Ar, N_2 and Xe; (C) correlation between gas permeance and pressure difference change across the membrane; and (D) calculated selectivity relative to N_2 of the membranes for the different gases (He, N_2, Ar, CO_2 and Xe). The permeance of N_2 across a 10 mm self-supporting BPs was found to be nearly 4 times higher than that of the hybrid membrane (979.82×10^{-10} mol m^{-2} s^{-1} Pa^{-1}).
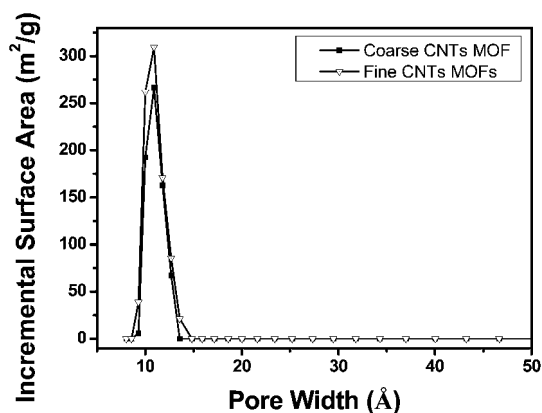
Fig. 4 Pore size distribution calculated from the BJH–BET model from N_2 adsorption for the two types of samples. Fine CNTs were shown to lead to slightly narrower pore size distribution, but no major changes were found confirming the homogeneity of the two structures.

atmospheric pressure (100 kPa) after the high-pressure test series and the average permeance was similar to that prior to high pressure testing, suggesting that the structure was able to support large pressure differentials without undergoing mechanical failure.

In addition, mixed gas separation tests were performed with a 50 : 50 N_2/CO_2 mixture. The N_2/CO_2 selectivity of the ZIF-8–CNT hybrid membranes was found to be of 6.9 confirming the selectivity based on single gas permeation and single gas adsorption. This non-Knudsen behaviour is attributed to the structure of ZIF-8 and to the strong adsorption of CO_2 onto non-fully crystallized 2-methyl imidazole weak bases present in the ZIF-8 structure. CO_2 gas was previously shown to very strongly

coordinate with these molecules remaining within ZIF-8 crystals.[16]

Conclusions

Defect-free hybrid CNT–ZIF-8 composite membranes were for the first time prepared by direct hydrothermal ZIF-8 growth within CNT BPs. The natural properties of CNT BPs including porosity and specific surface area are assets to successfully prepare robust, self-supported membranes able to sustain high pressures. Although fine CNTs lead to a higher gas absorbance, the permeation properties of the membranes were found to be very similar to that of pure ZIF-8 structures suggesting that the ZIF-8 growth within the interstitial pores of the BPs are constant regardless of the BP pore size. Furthermore, the high selectivity of N_2 over Xe demonstrates that the membranes were nearly defect-free and that the growth procedure was successful at creating an even interface between the CNTs and the ZIF-8 crystals. The low CO_2 selectivity over N_2 was shown to be related to very strong physisorption between the CO_2 and 2-methyl-imidazolidone molecules remaining within the ZIF-8 matrix. Mixed gas permeation tests confirmed this trend as nitrogen was found to permeate nearly 7 times faster than CO_2.

The good performance and stability of the novel MOF–CNT hybrid membranes make of these materials promising candidates in applications such as gas reforming, CO_2 capture from flue gas separation or steam purification. The future investigation of the nature of the interface between the MOFs and the reinforcing matrix, such as CNT BPs, is however fundamental to fully understand both growth mechanisms and gas separation performance.

Experimental section

CNT growth and BP fabrication

Two types of CNTs, referred to as fine (outer diameter of 10 nm) and coarse (outer diameter 40 nm), were grown via different CVD processes (Table 1). Fine CNTs were grown by first depositing an iron catalyst film (∼5 nm) onto a Si substrate bearing a thin (100–600 nm) SiO_2 layer. Acetylene (5%) in Helium was used as the carbon feedstock and heated to between 650 and 750 °C.[40] The coarse CNTs were produced by continuously injecting a ferrocene–acetylene mixture at a temperature of ∼700 °C which provides simultaneously both the carbon feedstock and iron catalyst for CNT growth. Substrates of quartz or silicon (with a thin SiO_2 layer) were used with no iron catalyst film. After growth the CNTs were scrapped from their wafers and suspended by sonication in propan-2-ol for 5 min up to 5 times at an initial temperature of −17 °C in a bath sonicator (50 W). BPs were formed by vacuum filtration (house vacuum line) of the CNTs suspension onto a poly(ethersulfone) membrane (0.2 µm pore size – Millipore) until completely dry. BPs formed solely from fine or coarse CNTs had an average surface apparent pore size of ∼25 nm and 50 nm, respectively (Table S2†).

ZIF 8 growth within the BPs

In a typical synthesis, a solid mixture of 1.078 g zinc chloride (>99% Merck), 0.972 g 2-methyl-imidazole (>99%, Aldrich) and 0.54 g sodium formate (>99%, Aldrich) were dissolved in 80 mL methanol (99.9%, Roth) under sonication. The BPs were placed at 90° on a hydrophobic (Teflon) support to avoid undesired ZIF-8 precipitation on the surface of the support, and immersed into the previous solution for 20 min. The BP and solution were then transferred to a 200 mL Teflon autoclave and heated in an oven at 100 °C for 24 h. After cooling, the membranes were washed with methanol and dried for 24 h in oven at 100 °C to remove residual humidity.

Characterization techniques

Scanning Electron Microscopy (SEM) was performed on a Zeiss Supra 55VP FEG SEM. Micrographs were taken at 3.5 mm working distance and under a 2 keV beam voltage (aperture 20 µm). The samples were carbon coated with a 1–2 nm thick layer. BET specific surface area measurements were performed on Micromeritics Tristar 3000 with N_2 at 77 K. The samples were degassed for 12 h at 100 °C prior to testing. X-ray diffraction (XRD) patterns were recorded on a PAN analytical PW3050/60 diffractometer with Cu Kα radiation (30 mA and 40 kV, wavelengths $\lambda = 0.1540598$ nm) at a scan rate of 0.5° min^{-1} with a step size of 0.02° from 5° to 50°. The adsorption of CH_4 and CO_2 was performed at 273 K while that of N_2 and H_2 were both obtained at 77 K (liquid N_2 temperature) using a Micromeritics ASAP 2420. The samples were degassed for 12 hours at 120 °C following a procedure described in ref. 22. SAXS experiments were performed on the SAXS/WAXS beamline at the Australian Synchrotron under the grant M2874 in March 2013. The camera length of this series of test was 0.96 m, corresponding to a scattering window of ∼0.010–0.7 Å^{-1} (D spacing range of 9–550 Å), wavelength of the collimated beam of 1.0332 Å, and beam size of 250 × 130 µm. The hybrid ZIF-8–CNT samples were sandwiched between two layers of Kapton tape and mounted onto perforated stainless steel plates. The high brilliance and coherence of the beam allowed for very short acquisition time (1 s). The energy of the beam was set at 11 keV for WAXS and 20 keV for SAXS experiments. The scattering from the Kapton tape was determined independently.

Gas permeation tests

Gas permeation experiments were performed on a single gas rig following a procedure described in ref. 26. The tests were performed by placing the membrane in an O-ring sealed (25.4 mm diameter) holder which separates a large upstream (feed – 14 L) vessel from a much smaller downstream (permeate – 15 mL) vessel. To ensure integrity of the O-ring seal, leak rate checks were performed with gas control impermeable poly(ethylene terephthalate) (PET) films.[26] The area of the exposed membranes was ∼5 mm^2. The hybrid ZIF-8–CNT membranes were sealed onto the PET film with an epoxy resin and cured at room temperature for at least 12 h. After loading the membrane, both the feed and permeate vessels were evacuated under vacuum (target pressure 0.1 kPa). The feed vessel was then isolated from both the vacuum and membrane holder, and filled to the target pressure (100, 150, 200, 300, 400, 500 and 600 kPa at ± 0.5 kPa) with analytical grade, dust-free, dehumidified gas. Prior to testing, the membrane was conditioned for 1 hour under vacuum to desorb any remaining water moisture or strongly adsorbed gas. For testing, the permeate side was isolated from vacuum. The feed vessel was opened to the permeate vessel via the membrane and the pressure rise in the permeate vessel monitored over time until equilibrium was reached. The feed pressure remained essentially constant due to its much larger volume compared to that of the permeate vessel. The membrane permeance was then determined from the pressure rise as a function of time.[26] All the tests were performed at controlled temperature (22 °C ± 1 °C). Mixed gas permeation tests were performed following a procedure previously detailed.[41] The binary gas separation via the ZIF-8 membrane was tested with a binary mixture of nitrogen and carbon dioxide (50 : 50 molar N_2/CO_2) at a flow rate of 150 mL min^{-1}. The pressures at the feed side and permeate side were kept at 151 and 101 kPa, respectively. Argon was used as the sweep gas and its flow rate was set at 100 mL min^{-1}. The gas composition was analyzed by a gas chromatograph (SRI 8610C gas chromatograph).

References

1 C. Sanchez, B. Julian, P. Belleville and M. Popall, *J. Mater. Chem.*, 2005, **15**, 3559–3592.

2 H. B. Tanh Jeazet, C. Staudt and C. Janiak, *Dalton Trans.*, 2012, **41**, 14003–14027.

3 Q. Song, S. K. Nataraj, M. V. Roussenova, J. C. Tan, D. J. Hughes, W. Li, P. Bourgoin, M. A. Alam, A. K. Cheetham, S. A. Al-Muhtaseb and E. Sivaniah, *Energy Environ. Sci.*, 2012, **5**, 8359–8369.

4 Z. Zhang, S. Xian, Q. Xia, H. Wang, Z. Li and J. Li, *AIChE J.*, 2013, 2195–2206.

5 J. M. Simmons, H. Wu, W. Zhou and T. Yildirim, *Energy Environ. Sci.*, 2011, **4**, 2177–2185.

6 S. K. Nune, P. K. Thallapally, A. Dohnalkova, C. Wang, J. Liu and G. J. Exarhos, *Chem. Commun.*, 2010, **46**, 4878–4880.

7 D. Zacher, O. Shekhah, C. Woll and R. A. Fischer, *Chem. Soc. Rev.*, 2009, **38**, 1418–1429.

8 J. Yao, D. Dong, D. Li, L. He, G. Xu and H. Wang, *Chem. Commun.*, 2011, **47**, 2559–2561.

9 Z. Y. Lu, H. Xing, R. Sun, J. F. Bai, B. S. Zheng and Y. Z. Li, *Cryst. Growth Des.*, 2012, **12**, 1081–1084.

10 L. Fan, M. Xue, Z. Kang, H. Li and S. Qiu, *J. Mater. Chem.*, 2012, **22**, 25272–25276.

11 L. Li, J. Yao, R. Chen, L. He, K. Wang and H. Wang, *Microporous Mesoporous Mater.*, 2013, **168**, 15–18.

12 Y.-n. Wu, F. Li, H. Liu, W. Zhu, M. Teng, Y. Jiang, W. Li, D. Xu, D. He, P. Hannam and G. Li, *J. Mater. Chem.*, 2012, **22**, 16971–16978.

13 D. J. Lee, Q. Li, H. Kim and K. Lee, *Microporous Mesoporous Mater.*, 2012, **163**, 169–177.

14 A. Centrone, Y. Yang, S. Speakman, L. Bromberg, G. C. Rutledge and T. A. Hatton, *J. Am. Chem. Soc.*, 2010, **132**, 15687–15691.

15 F. Hinterholzinger, C. Scherb, T. Ahnfeldt, N. Stock and T. Bein, *Phys. Chem. Chem. Phys.*, 2010, **12**, 4515–4520.

16 G. Xu, J. Yao, K. Wang, L. He, P. A. Webley, C.-s. Chen and H. Wang, *J. Membr. Sci.*, 2011, **385–386**, 187–193.

17 M. Silva Pinto, C. Sierra-Avila and J. Hinestroza, *Cellulose*, 2012, **19**, 1771–1779.

18 M. Rose, B. Böhringer, M. Jolly, R. Fischer and S. Kaskel, *Adv. Eng. Mater.*, 2011, **13**, 356–360.

19 R. Ostermann, J. Cravillon, C. Weidmann, M. Wiebcke and B. M. Smarsly, *Chem. Commun.*, 2011, **47**, 442–444.

20 P. Pachfule, B. K. Balan, S. Kurungot and R. Banerjee, *Chem. Commun.*, 2012, **48**, 2009–2011.

21 L. F. Dumée, K. Sears, J. Schütz, N. Finn, C. Huynh, S. Hawkins, M. Duke and S. Gray, *J. Membr. Sci.*, 2010, **351**, 36–43.

22 L. Dumee, M. R. Hill, M. Duke, L. Velleman, K. Sears, J. Schutz, N. Finn and S. Gray, *J. Mater. Chem.*, 2012, **22**, 9374–9378.

23 L. F. Dumée, K. Sears, B. Marmiroli, H. Amenitsch, X. Duan, R. Lamb, D. Buso, C. Huynh, S. Hawkins, S. Kentish, M. Duke, S. Gray, P. Innocenzi, A. J. Hill and P. Falcaro, *Carbon*, 2013, **51**, 430–434.

24 L. Dumée, V. Germain, K. Sears, J. Schütz, N. Finn, M. Duke, S. Cerneaux, D. Cornu and S. Gray, *J. Membr. Sci.*, 2011, **376**, 241–246.

25 J. Wu, K. Gerstandt, M. Majumder, X. Zhan and B. J. Hinds, *Nanoscale*, 2011, **3**, 3321–3328.

26 K. Sears, L. Dumee, J. Schuetz, M. She, C. Huynh, S. Hawkins, M. Duke and S. Gray, *Materials*, 2010, **3**, 127–149.

27 K. S. Park, Z. Ni, A. P. Côté, J. Y. Choi, R. Huang, F. J. Uribe-Romo, H. K. Chae, M. O'Keeffe and O. M. Yaghi, *Proc. Natl. Acad. Sci. U. S. A.*, 2006, **103**, 10186–10191.

28 S. R. Venna, J. B. Jasinski and M. A. Carreon, *J. Am. Chem. Soc.*, 2010, **132**, 18030–18033.

29 M. Zhu, J. B. Jasinski and M. A. Carreon, *J. Mater. Chem.*, 2012, **22**, 7684–7686.

30 A. Cao, C. Xu, J. Liang, D. Wu and B. Wei, *Chem. Phys. Lett.*, 2001, **344**, 13–17.

31 L. Dumée, A. Thornton, K. Sears, J. Schütz, N. Finn, S. Spoljaric, R. Shanks, C. Skourtis, M. Duke and S. Gray, *Progress in Natural Science: Materials International*, 2012, **22**, 673–683.

32 J. Cravillon, C. A. Schröder, R. Nayuk, J. Gummel, K. Huber and M. Wiebcke, *Angew. Chem., Int. Ed.*, 2011, **50**, 8067–8071.

33 B. Assfour, S. Leoni and G. Seifert, *J. Phys. Chem. C*, 2010, **114**, 13381–13384.

34 B. Zheng, M. Sant, P. Demontis and G. B. Suffritti, *J. Phys. Chem. C*, 2011, **116**, 933–938.

35 D. Fairen-Jimenez, S. A. Moggach, M. T. Wharmby, P. A. Wright, S. Parsons and T. Düren, *J. Am. Chem. Soc.*, 2011, **133**, 8900–8902.

36 Y. Pan and Z. Lai, *Chem. Commun.*, 2011, **47**, 10275–10277.

37 A. Huang, H. Bux, F. Steinbach and J. Caro, *Angew. Chem., Int. Ed.*, 2010, **49**, 4958–4961.

38 C. A. Scholes, S. E. Kentish and G. W. Stevens, *Recent Pat. Chem. Eng.*, 2008, **1**, 52–66.

39 H. Bux, F. Liang, Y. Li, J. Cravillon, M. Wiebcke and J. r. Caro, *J. Am. Chem. Soc.*, 2009, **131**, 16000–16001.

40 C. P. Huynh and S. C. Hawkins, *Carbon*, 2010, **48**, 1105–1115.

41 C. Zeng, L. Zhang, X. Cheng, H. Wang and N. Xu, *Sep. Purif. Technol.*, 2008, **63**, 628–633.